Visualization of Cardiac Parasympathetic Nervous Activity in Form

Kiyoko Yokoyama* and Noriaki Kamiya

Graduate School of Design and Architecture, Nagoya City University, 2-1-10 Kitachikusa, Chikusa-ku, Nagoya 464-0083, Japan
E-mail address: yokoyama@sda.nagoya-cu.ac.jp

(Received September 22, 2008; Accepted March 10, 2009)

In the field of medical science, the invisible real forms of organs may be visualized using advanced technology. Few studies have visualized physiological condition in form. The purpose of this study is to visualize cardiac parasympathetic nervous activity in form. The power of high-frequency component of R-R interval time series derived from ECG (HF: 0.15–0.4 Hz) is an index of cardiac parasympathetic nervous activity. This index is visualized as a form. To realize real-time and continuous visualization of cardiac parasympathetic nervous activity, we developed a new method for calculation of HF power. The estimated accuracy of this method for calculating HF power was the same as in the conventional method. From an experiment comparing the various kinds of image, visualization using an apple with a facial expression was considered to have a related physiological and psychological relaxation effect.
Key words: Heart Rate Variability, Cardiac Parasympathetic Nervous Activity, Power Spectrum Analysis, High Frequency Component, Visualization

1. Introduction

In the field of medical science, the invisible real forms of organs may be visualized using advanced technology (Swenberg, 1988). Few studies have visualized physiological condition as a form. One such example is visualization of muscle activity by a moving CG avatar (Matsukawa *et al.*, 2007; Choi *et al.*, 2007). The other example is indicating the heart rate by music (Yokoyama *et al.*, 2002). But it seems there is no example in which autonomic nervous balance is visualized in form. The purpose of this study is to visualize cardiac parasympathetic nervous activity in form.

The heart rate time series derived from electrocardiograph (ECG) is fluctuated by the effect of cardiac autonomic nervous control. A heart rate time series reportedly contains well-defined rhythms, which have been successfully shown to contain physiological information (Sayers, 1973; Akselrod *et al.*, 1981). The major components of this fluctuation are Mayer rhythm and respiratory sinus arrhythmia (RSA). The Mayer rhythm reflects the systolic rhythm of speripheral blood vessels. The band-width of this rhythm is from 0.04 to 0.15 [Hz]. This is called the low-frequency component (LF). Its physiological interpretation is still controversial. Both sympathetic and parasympathetic contributions can be involved (Cerutti *et al.*, 1995). The frequency of RSA is synchronized with the respiratory frequency. The frequency of this rhythm is from 0.15 to 0.4 [Hz], and this frequency is called the high-frequency component (HF). This rhythm is due to the intrathoracic pressure changes and mechanical variations caused by the breathing activity. It is mediated by the vagus nerve on the heart (Cerutti *et al.*, 1995). These components are used as indices of autonomic nervous balance. The power of HF is an index of cardiac parasympathetic nervous activity, and the ratio of LF power to HF power is related to sympathetic nervous activity (Montano *et al.*, 1994; Task Force of the European Society of Cardiology and the North American Society of Pacing and Electrophysiology, 1996).

In this study, HF power, which is an index of cardiac parasympathetic nervous activity, is visualized in form. HF power is calculated from the power spectrum in general. The power spectrum is calculated using Fourier transform, the maximum likelihood method or auto regressive model etc. (Kay and Marple, 1981). These methods are not appropriate for real-time calculation, because they require complex calculation procedures. To realize real-time and continuous visualization of cardiac parasympathetic nervous activity, we developed a new method for calculation of HF power. This method can calculate HF power continuously using a short time window.

To visualize the cardiac parasympathetic nervous activity reflected in the HF power of heart rate time series in form, it becomes possible to monitor the unsteady change of autonomic nervous activity caused by various actions in daily life. This monitoring technique can be used for daily health care management, relaxation treatment, stress or fatigue monitoring and so on.

2. Algorithm for Calculation of HF Power

A time series of R-R intervals was used for analysis. R-R interval is the interval of two-neighboring R peaks in the ECG signal. R peak corresponds to the depolarization of the ventricles. HF power is estimated from subtraction of the neighboring two extremals in the R-R interval time series. The procedure is described as follows.

1) Detection of an extremal

A k-th extremal T_k at point P_k is equal to $r(i)$ in Eq. (2),

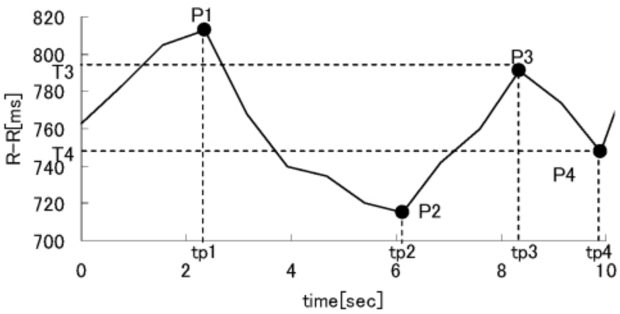

Fig. 1. R-R interval time series. Points P_1 to P_4 are extremals. From tp_1 to tp_4 are the times at extremal. T_3 and T_4 are the extremals contained in HF wave.

while $\{r(i), i = 1, 2, \ldots, N\}$ satisfies Eq. (1):

$$(r(i) - r(i-1))(r(i+1) - r(i)) < 0 \quad (1)$$

$$T_k = r(i) \ \ (k = 1, 2, \ldots, M) \quad (2)$$

where $r(i)$ is the i-th R-R interval. The R-R interval presents the interval of two neighboring heart beats in ECG. N is the number of R-R intervals and M is the number of extremals.

2) Calculation of the power of HF

HFP_k in Eq. (3) shows the local power derived from the two neighboring extremals, T_{k+1} and T_k, which are the $(k+1)$-th and k-th extremals. $|T_{k+1} - T_k|$ is the peak-to-peak value of the wave containing the points P_{k+1} and P_k:

$$\mathrm{HF}P_k = (|T_{k+1} - T_k|/2)^2. \quad (3)$$

3) Detection of high-frequency component

The frequency band of HF is 0.15 to 0.4 Hz. The period of signal fluctuating with 0.15 Hz is 6.7 sec. The time at P_k is described as tp_k. The interval of tp_{k+1} and tp_k is the half period of a wave containing P_{k+1} and P_k. If the interval of tp_{k+1} and tp_k is not over 3.35 [sec], the wave containing P_{k+1} and P_k is detected as HF (Eq. (4)).

$$2(tp_{k+1} - tp_k) \leq 6.7(\mathrm{sec}). \quad (4)$$

An example of the R-R interval time series and the points observing extremal (•) are presented in Fig. 1. The abscissa shows the time and the ordinate indicates the R-R intervals. T_k is the k-th extremal. The time at observing extremal is described as $tp_k (k = 1, 2, 3, 4)$. In this figure, the interval of the neighboring extremals P_2 and P_1 is 4 [sec], that is $(tp_2 - tp_1)$. This time interval is longer than $6.7/2 = 3.35$ [sec]. The time series from tp_1 to tp_2 is the part of the low-frequency waveform. In this case, the power of HF is output as zero. The interval of neighboring extremals P_3 and P_4 is 1.6 [sec], which is less than 3.35 [sec]. P_3 and P_4 are part of the high-frequency component. The power of this HF wave is $(|T_4 - T_3|/2)^2$.

3. Evaluation of Proposed Method

Calculation accuracy of the proposed algorithm was evaluated using a simulated time series. In this analysis, sinusoidal time series with the amplitude one, whose frequency components varied randomly at each period, were generated. The frequency band of the component is 0.04 to 0.45 [Hz]. The result is shown in Fig. 2. The simulated R-R interval time series is shown above, with the frequency change of this time series in the middle, and the power calculated using the proposed method indicated below. In this power, the positive value shows the power estimated as HF, and the negative value shows the power estimated as LF. The horizontal line at 0.15 [Hz] in the middle shows the threshold between LF and HF. Dotted vertical lines show the position detecting low-frequency components. At the waveform position with frequency exceeding the threshold frequency, the power is calculated as positive, which means HF.

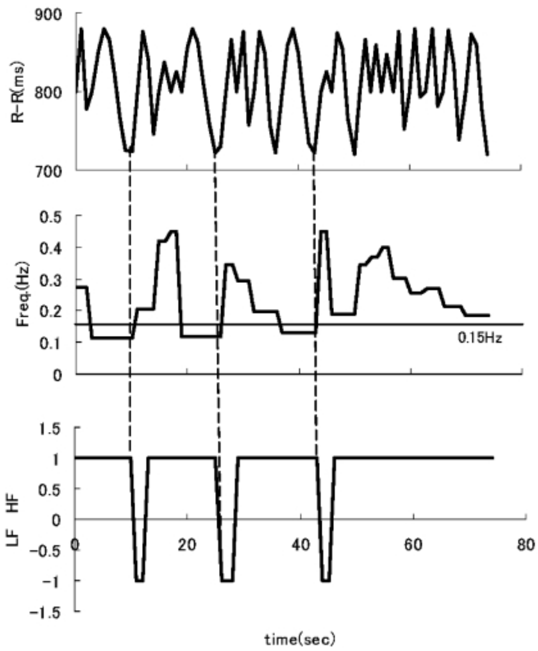

Fig. 2. Detection of HF wave. Above: R-R intervals (simulation). Middle: Frequency of R-R interval time series. Below: Result of detection. 1: HF, −1: LF.

4. Evaluation Using Measured R-R Interval Data

The proposed method was compared with conventional methods such as the fast Fourier transform (FFT) (Cooley and Tukey, 1965), auto regressive (AR) method (Akaike, 1969) and wavelet transform (Gabor Transform) (Akay and Mello, 1997).

FFT is a method for efficiently computing the discrete Fourier transform of time series. The power spectral density function calculated from the discrete Fourier transform is represented by Eq. (5).

$$P_{\mathrm{FFT}}(f) = \left| \sum_{t=1}^{N} r(t) \exp(-j2\pi f t \Delta t) \right|^2. \quad (5)$$

In this equation, $r(t)$ is the time series of R-R intervals, N is the number of data (N is the power of two in FFT method), j is the imaginary unit, f is the frequency and Δt is the sampling interval of the time series.

To calculate the power spectral density function using AR method, an AR model is estimated from the time series. The AR model represented by the following equation is the

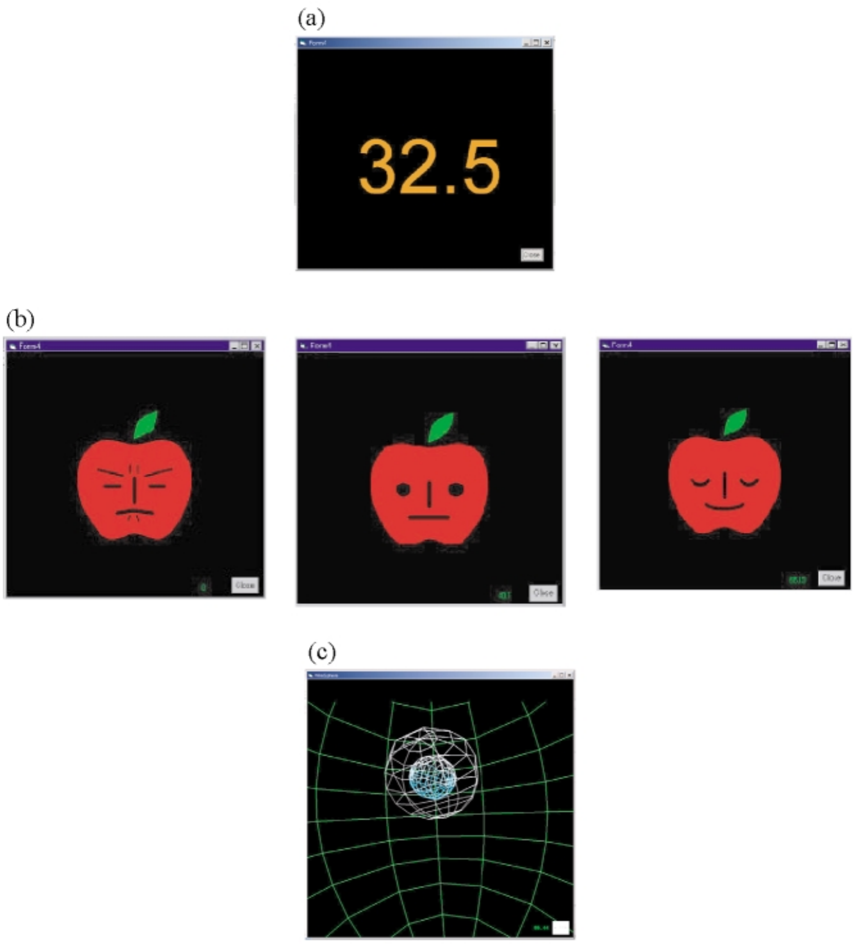

Fig. 3. Images displayed to participants. (a) Numeric character representing HF power; Numeric. (b) Apple representing HF power with facial expression; Apple. (c) Wire-frame sphere; Sphere1 (Speed of animated motion is according to the HF power); Sphere2 (Speed of animated motion is in inverse proportion to HF power).

linear prediction model of time series:

$$r(t) = \sum_{k=1}^{p} a(k) r(t-k) + Z(t) \tag{6}$$

where $r(t)$ is the time series of R-R intervals, $a(k)$ is the linear prediction coefficient, p is the order of the autoregressive process, and $Z(t)$ is the prediction error, which is the white noise. The optimal order of the autoregressive process is selected as the minimized the final prediction error (FPE) described below:

$$\mathrm{FPE}(k) = Z_{sd}^2 \frac{N+k}{N-k}. \tag{7}$$

Z_{sd}^2 is the variance of $Z(t)$ and N is the number of data.

The power spectral density function ($P_{AR}(f)$) is described in Eq. (8).

$$P_{AR}(f) = \frac{Z_{sd}^2}{\left|1 - \sum_{k=1}^{p} a(k) \exp(-j2\pi f k)\right|^2}. \tag{8}$$

In this equation f is the frequency.

Wavelet transform is one of the popular time-frequency analysis methods. This method is useful for the analysis of non-stationary time series. Wavelet transform provides a flexible time-frequency window according to observing frequency. Gabor transform is one of the wavelet transforms. The power spectral density function derived from the Gabor transform is described in below:

$$P_{wt}(f) = \left| \sum_{t=1}^{N} \frac{\exp\left(-\frac{(t-b)^2}{4f}\right)}{2\sqrt{\pi f}} \exp(-j2\pi f t \Delta t) \right|^2. \tag{9}$$

Gaussian function localizes the Fourier transform of f around $t = b$ in the Gabor transform.

Next, 170 measured R-R interval time series with 3-minute long were analyzed. The area of the power spectral density function with 0.15 to 0.4 [Hz] is defined as the HF power in FFT and AR methods. A time window with 20 [sec] width is used to calculate power by the wavelet transform. The average of the powers derived from the moving window 1 [sec] interval is defined as the HF power in the wavelet transform.

The correlation coefficients of the proposed method and other methods are shown in Table 1. A large correlation coefficient is presented in the AR model and in the wavelet transform. The accuracy of estimation of the HF power is the same as with the conventional methods.

Table 1. Correlation coefficients between proposed method and conventional method. AR: auto regressive model, FFT: fast Fourier transform, Gabor: wavelet transform (Gabor transform).

Method	AR	FFT	Gabor
r	0.98	0.92	0.98

The relationship between the ratio of amplitude of HF to LF (HFA/LFA) and error rate of estimation of HF power was analyzed. In this simulation analysis, a time series is generated from Eq. (10). In Eq. (10), LFA and HFA are the amplitude of LF and HF, respectively. LFF and HFF are the frequency of LF and HF. The sampling rate is described as the delta t. 1000 simulated data were analyzed.

$$r(t) = \mathrm{LFA}\sin(2\pi\,\mathrm{LFF}t\Delta t) + \mathrm{HFA}\sin(2\pi\,\mathrm{HFF}t\Delta t). \quad (10)$$

Table 2 shows the high calculation accuracy, when HFA/LFA is larger than 0.4. Almost all data with HFA/LFA larger than 0.4 had a small error rate of less than 0.1. The average error rate of these data, whose HFA/LFA is larger than 0.4, was 8%. The dominant frequency of HF (HFF) and dominant frequency of LF (LFF) were used for calculation of evaluation parameter of the estimation accuracy. The new evaluation parameter is (HFA/LFA-(HFF-LFF)). The average error rate of this data, with (HF/LF-(HFF-LFF)) larger than 1.0, is 5%.

5. Experiment for Evaluating Effects of Visualizing Cardiac Parasympathetic Nervous Activity in Form

5.1 Visualizing method

The R-R interval time series were measured using a portable heart rate monitor (LRR-03 GMS). The measured R-R interval was transmitted to the PC through RS-232C. HF power was calculated from the R-R interval time series. These HF powers were reflected in the CG images.

A moving average with 20-beat window width was applied to the time series of HF powers. This moving average method can prevent any abrupt change of the image. To avoid personal differences, the HF power was normalized by measuring data while sitting at rest.

Three kinds of image were prepared. In Fig. 3, (a) is a numeric character with large font-colored orange (Numeric). (b) shows three apples with facial expressions (Apple). (c) shows a wire-frame sphere model by 3-D computer graphics (Sphere1 and Sphere2).

The value of (a) reflects the HF power. If the power is large, the cardiac parasympathetic nervous activity is large, and the value is thereby increased. A face in (b), in which the three aspects are smile (large HF power), neutral (medium HF power) and pain (small HF power), was prepared. In sphere1, the speed of the animated motion of the sphere was increased according to the HF power. In sphere2, the speed of the animated motion of the sphere was decreased according to the HF power.

5.2 Experimental method

The volunteer participants in this experiment were 19 (14 men and 5 women) healthy students aged 18 to 24 years old (21.4 ± 1.4; average ±SD). The relationship between emotional stress and heart rate variability was independent of gender (Dishman *et al.*, 2000). So, it is considered that the unequal number of participants' gender did not affect the experimental results. A photo of one participant during the experiment is shown in Fig. 4. The protocol of the experiment is shown in Fig. 5. Each participant was given sufficient explanation of the experiment and gave written consent. In the first three minutes, R-R intervals were measured to use the normalization procedure. Participants sat for one minute, then performed mental arithmetic for 3 minutes and watched a cartoon reflecting the HF power or relaxation video for three minutes. The numeric character, an apple, two kinds of animation of wire-frame sphere and relaxation video without reflection of the HF power, were compared. The relaxation video was about animals. The order of displaying the content was determined randomly.

Fig. 4. A photo of one participant during the experiment.

5.3 Results and discussion

The average of the HF powers while sitting at rest for three minutes and the average of the HF powers while watching images for three minutes were calculated. The average and standard deviation of these values derived from sitting at rest for three minutes while watching four kinds of images reflecting HF power. Watching the relaxation video served to standardize the values. In this case, the average was zero, and the standard deviation was one in each participant.

The relationship between the condition (sitting rest, numeric character, apple, sphere1, sphere2, relaxation video) and the HF power averaging for three minutes is presented in Fig. 6. The black circles show the average of 14 participants, the top of the bar indicates the maximum values among 14 participants, and the bottom of the bar shows the minimum value. HF power while sitting at rest was significantly ($p < 0.01$) less than the other conditions. The HF power while watching the apple was significantly greater than watching sphere1 ($p < 0.01$). In this result, the image reflecting HF power has the effect of increasing HF power. It is considered that the images reflecting HF power can activate cardiac parasympathetic nervous activity.

Subjective evaluations were performed. As for the likability of the image, the relaxation effect, fatigue, sleepiness and suiting one's mood were evaluated. The participants were required to answer the degree of their agreement

Table 2. Histogram of HFA/LFA. >0.1: Error rate larger than 0.1, <=0.1: Error rate less than 0.1.

	0–0.2	0.2–0.4	0.4–0.6	0.6–0.8	0.8–1.0	1.0–1.2	1.2–1.4	1.4–	Subtotal (>0.4)	Total
>0.1	96	55	17	26	11	8	4	2	68	219
<=0.1	0	11	60	70	83	83	76	398	770	781

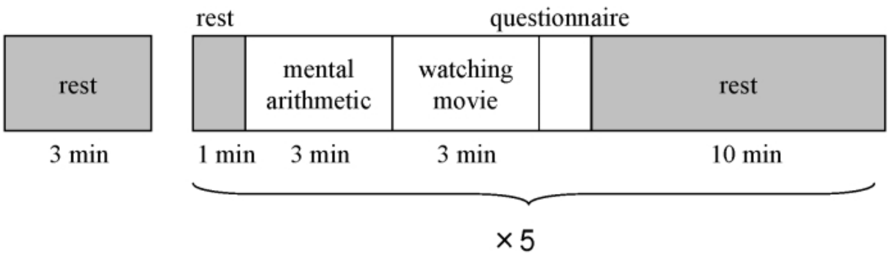

Fig. 5. Experimental protocol.

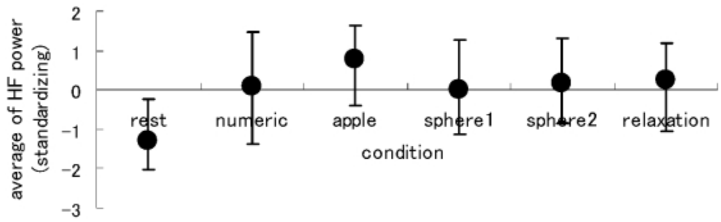

Fig. 6. Relationship between condition and average of HF power.

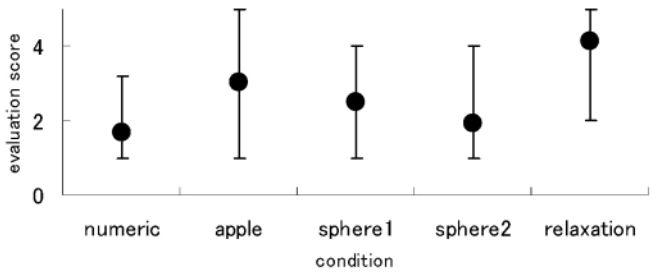

Fig. 7. Relationship between image and evaluation score of relaxation effect.

with each question: “Very much agree”, “Agree”, “yes and no (neutral)”, “Do not agree” and “Completely disagree.” In the questionnaire, a visual analogue scale (VAS) was used. “Completely disagree” was assigned 1 and “Very much agree” was assigned 5 for statistical analysis.

One-way analysis of variance (ANOVA) was applied to all questions to analyze the significance of the variance among images. The relaxation effect varied significantly ($p < 0.05$). In Fig. 7, the average answer about the relaxation effect is shown while watching the numerical character, apple, sphere1, sphere2 and relaxation video. The relaxation effect of the relaxation video was the very highest among other images. The relaxation effect of the apple was larger than sphere2, in which the velocity of motion (animation) is decreased according to the HF power. The apple image is considered to offer psychological relaxation.

6. Conclusion

The purpose of this study was to visualize cardiac parasympathetic nervous activity in form. Cardiac parasympathetic nervous activity was estimated from the heart rate time series in real time. An estimation method was proposed in this study. The estimated accuracy of this method was the same as in the conventional method, such as the AR method and the wavelet method. This parameter called HF power, which is reflected in the cardiac parasympathetic nervous activity, was visualized using various images. From the experiment comparing the various kinds of image, visualization using the apple with facial expressions was considered to have a related physiological and psychological relaxation effect.

In future study, sphygmography will be used to estimate HF power for application in daily life. The sphygmography can be measured without attaching electrodes. It can be measured using photoelectric transducer, which is a simple and convenient sensor. The HF power of sphygmography calculated from the complex demodulation method reportedly contains the same information as the HF power derived form the R-R interval time series (Sakakibara *et al.*, 2008).

References

Akaike, H. (1969) Power spectrum estimation through autoregressive model fitting, *J. Annals of the Institute of Statistical Mathematics*, **21**(1), 407–419.

Akay, M. and Mello, C. (1997) Wavelets for biomedical signal processing, in *Proc. of Engineering in Medicine and Biology Society, 19th Annual Int. Conf. of the IEEE*, **6**, pp. 2688–2691.

Akselrod, S., Gordon, D. S., Ubel, F. A. *et al.* (1981) Power spectrum analysis of heart rate fluctuations: a quantitative probe of beat-to-beat cardiovascular control, *Science*, **213**, 213–220.

Cerutti, S., Bianchi, A. M. and Mainardi, L. T. (1995) Spectral analysis of the heart rate variability signal, in *Heart Rate Variability* (eds. M. Malik and A. J. Camm), pp. 63–74.

Choi, W., Isaka, T., Sakata, M., Tsuruta, S. and Hachimura, K. (2007) Quantification of dance movement by simultaneous measurement of body motion and biophysical, *Int. Jour. of Automation and Computing*, **4**(1), 1–7.

Cooley, J. W. and Tukey, J. W. (1965) An algorithm for the machine calculation of complex Fourier series, *Math. Comput.*, **19**, 297–301.

Dishman, R. K., Nakamura, Y., Garcia, M. E., Thompson, R. W., Dunn, A. L. and Blair, S. N. (2000) Heart rate variability, trait anxiety, and perceived stress among physically fit men and women, *Int. J. Psychophysiol.*, **37**(2), 121–133.

Kay, S. M. and Marple, S. L. (1981) Spectrum analysis—A modern perspective, in *Proc. of the IEEE*, **69**(11), 1380–1419.

Matsukawa, T., Umetani, T. and Yokoyama, K. (2007) Development of health monitoring system based on three-dimensional imaging using bio-signals and motion data, in *Proc. of 29th Annual Int. Conf. IEEE, Engineering in Medicine and Biology*, pp. 1523–1527.

Montano, N., Ruscone, T. G., Porta, A., Lombardi, F., Paganii, M. and Malliani, A. (1994) Power spectrum analysis of heart rate variability to assess the changes in sympathovagal balance during graded orthostatic tilt, *Circulation*, **90**, 1826–1831.

Sakakibara, M., Kanematsu, T., Yasuma, F. and Hayano, J. (2008) Impact of real-world stress on cardiorespiratory resting function during sleep in daily life, *Psychophysiology*, **45**(4), 667–670.

Sayers, B. A. (1973) Analysis of heart rate variability, *Ergonomics*, **16**, 85–97.

Swenberg, C. E. (1988) *Imaging Techniques in Biology and Medicine*, Academic Press, N.Y.

Task Force of the European Society of Cardiology and the North American Society of Pacing and Electrophysiology (1996) Heart rate variability—Standards of measurement, physiological interpretation, and clinical use, *Circulation*, **93**, 1043–1065.

Yokoyama, K., Ushida, J., Sugiura, Y., Mizuno, M., Mizuno, Y. and Takata, K. (2002) Heart rate indication using musical data, *Trans. on IEEE Biomedical Engineering*, **49**(7), 729–733.